

Comparison of SPR and T-MOKE Effects in Magneto-optic Plasmonic Nanostructures

Conrad Rizal,^{1,2,3, a)} Pavel O Kapralov,^{4, b)} Daria Ignatyeva,^{4,5, c)} Vladimir Belotelov,^{4,5, d)} and Simone Pisana^{1, e)}

¹⁾ *Department of Electrical Engineering & Computer Science, York University, 4700 Keele Street, Toronto, ON, M3J 1P3, Canada*

²⁾ *SeedNanoTech International Inc., 4 Howell St, Brampton, ON, L6Y3J6, Canada*

³⁾ *GEM Systems Inc., 135 Spy Crt, Markham, ON, L3R 5H6, Canada*

⁴⁾ *Russian Quantum Center, Novaya Street, Skolkovo, Moscow, 143025, Russia*

⁵⁾ *Faculty of Physics, Lomonosov Moscow State University, Leninskie Gory, Moscow, Russia*

(Dated: 10 October 2019)

Abstract: In this Letter, we report on the response of surface plasmon resonance (SPR, Reflectance vs. incident angle) and transverse magneto-optic Kerr effect (T-MOKE vs. incident angle) in two different magneto-optic-plasmonic (MOP) configurations: Ti/Au/Co/Au (Configuration A) and Ti/Ag/Co/Au (Configuration B) at the excitation wavelength of 780 nm in air. Configuration A includes a 35 nm Au layer and configuration B includes a 35 nm Ag layer. Both configurations consist of a thin (4 or 8 nm) Co magneto-optic layer and showed an enhancement of the T-MOKE signal over the SPR signal. Configuration B showed higher SPR and T-MOKE response over configuration A, possibly due to the low loss and higher plasmonic properties of Ag over Au. The T-MOKE based sensor shows improvements in quality factor by over 2X compared to that of SPR. The magneto-optic SPR sensitivity of the sensor obtained shows an improvement by 3X over the SPR sensitivity, and this can be further improved by suitably modifying the configuration. These results are of importance to the development of enhanced MOP/plasmonic sensors.

PACS numbers: 75.70.Cn, 78.20.Ls, 85.70.Sq

Keywords: Au/Co/Au, Ag/Co/Au, multilayers, SPR, T-MOKE, sensors

I. INTRODUCTION

Magneto-optic-plasmonic (MOP) structures - a new class of devices that have been considered essential for enhanced surface plasmon resonance (SPR) and transverse magneto-optic Kerr effect (T-MOKE) responses useful in sensing applications¹⁻⁸. In this Letter, we report the reflectance and T-MOKE effects shown by Ti/Au/Co/Au and Ti/Ag/Co/Au structures and compare the performance at a wavelength, $\lambda = 780$ nm. For simplicity in terms of fabrication, assembly, and handling purposes, the *Kretschmann* geometry is used for exciting SPRs (see, ^{4,9-13} for details).

In the *Kretschmann* geometry, the surface plasmons are excited at the interface of a metallic multilayer and air (the probed medium when used for sensing applications). These surface plasmons are oscillations of the electrons, and they travel with distinct frequency and wave vector (longitudinal wave) along with the interface. The displacement of the surface plasmons with respect to positive ion is parallel to the propagation, and they are excited using incident optical radiation at a specific wave-

length, and at an oblique angle for wave-vector matching, p-polarized light excites surface plasmons and form surface plasmon polaritons (SPP).

The surface plasmon waves are confined at the surface of the sensor, and this confinement makes these waves very sensitive to the dielectric environment within the region the evanescent wave field extends. The addition of the magnetic material yields a magneto-optic enhancement, which is a unique feature of T-MOKE configuration. SPR sensors with a magnetic layer are also referred to magneto-optic SPR (MO-SPR) sensors.

Most of the previous studies have been focused on studying reflectance and T-MOKE response in bilayers of Au/Co, Au/Fe, Ag/Co or Ag/Fe, where the Au or Ag act as the plasmonic layer and Co or Fe as the magneto-optic component of the MOP configuration. In the present work, we compare the performance between the Au-rich (Ti/Au/Co/Au, Configuration A) and Ag-rich (Ti/Ag/Co/Au, Configuration B) multilayers. The response curves are measured in air as the sensing medium and compared to models, demonstrating improved performance of the Ag-rich sensors over Au-rich sensors. The configurations explored here differentiate themselves in two ways: (i) they include the effect of the adhesion layer, which although introduces losses it is often necessary for reliable fabrication, (ii) they are composed of thin plasmonic layers on the side of the sensing surface, which is opposite to the typical arrangement.

^{a)} Electronic mail: conrad.rizal@seednanotech.com

^{b)} Electronic mail: kapralov.pavel@mail.ru

^{c)} Electronic mail: daria.ignatyeva@gmail.com

^{d)} Electronic mail: v.i.belotelov@ya.ru

^{e)} Electronic mail: simone.pisana@lassonde.yorku.ca

II. MATERIALS AND METHODS

The magneto-optic-plasmonic (MOP) structures were designed using MATLAB and COMSOL Multiphysics simulation tools based on Fresnel reflections and the transfer matrix method outlined in¹⁴. The complex optical constants of all the materials were obtained from¹⁵. The optical constants are refined using the experimental results by fitting the data to the model. The optimized multilayer structure consisted of a 2 nm Ti as an adhesion layer, an internal plasmonic layer of Ag/Au, a magneto-optic Co layer, and an external plasmonic Au layer (see, Fig 1). The outer 10 nm Au also works as a capping layer for both the configurations (Configurations A and B). The total thickness of the multilayer was chosen/optimized to match the thickness of a single Au layer that gives the best SPR result.

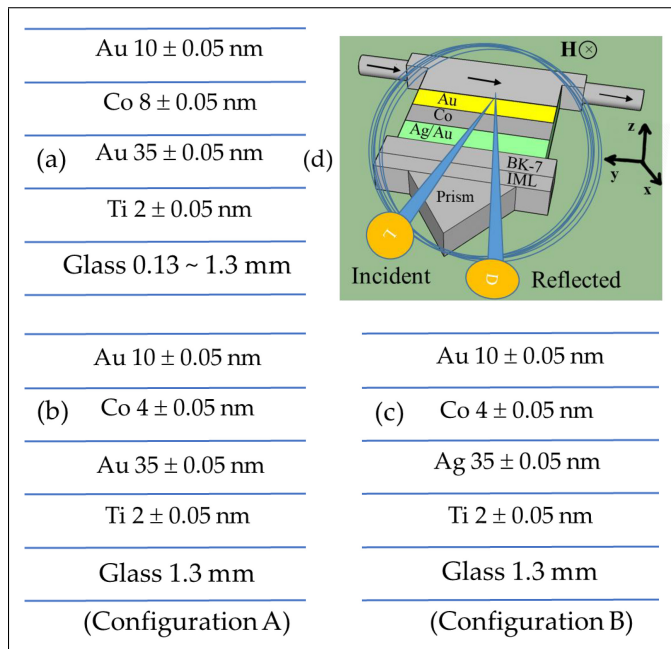


FIG. 1. Magneto-optic-plasmonic configurations (a,b) Ti/Au-Co-Au and (c) Ti/Ag-Co-Au (d) Excitation schematic.

The samples were deposited using electron beam evaporation on BK7 glass. The multilayered films were deposited in one deposition run without breaking vacuum. The characterization performed at the time of fabrication was the verification of the film thickness via atomic force microscopy. The deposition rates were 1.2, 0.7, 0.5, and 0.7 Å/s for Ti, Au, Ag, and Co, respectively. The layer thickness with the allowable deposition tolerance of the sample are shown in Fig 1. Prior microstructure and magnetic studies on the samples prepared using e-beam evaporation have shown relatively good crystallinity, sharp interfaces and remanent magnetization in-plane, parallel to the Au layer¹⁰.

For the reflectance and T-MOKE characterization a laser diode (Thorlabs QL7816S-B-L, Germany) was used

to generate a linearly p-polarized light. The laser wavelength was tuned via temperature control of the module with an accuracy of 0.01 K and was controlled using a spectrometer (Horiba HR-320, Japan). The optical radiation was then collimated and focused using spherical and cylindrical lenses with $f=150$ mm and 18 mm, respectively. The reflected radiation was collected using a monochrome CMOS matrix camera (IDS UI-3360CP-M-GL) having 2048 X 1088-pixel screen (11.264 mm X 5.984 mm screen dimension), yielding a $5.5 \mu\text{m}$ pixel size.

The MOP samples were placed inside an electromagnet ($H \cong 30$ mT) with the inter-polar gap of 30 mm in transverse Kerr geometry (orthogonal to the plane of the Fig. 1d), and controlled via LabVIEW program to record the real-time reflectance angular spectra as well as the T-MOKE spectra. Air with 30% humidity was blown at atmospheric pressure and room temperature of 21.6°C . As shown in Figure 1(d), the optical radiation is incident on the prism with a roughly 3° diverging beam centred around the resonant surface plasmon excitation angle. For both reflectance and T-MOKE effect, angular interrogation is used with the incident angle varied between 39 to 43° as collected by the CMOS camera. For the T-MOKE study, the multilayers were magnetized in the transverse direction (as indicated by the direction of H in the figure). For further detail and measurement methods, see⁴.

III. RESULTS

Figure 2 shows the theoretical SPR curves fitted to the experimental data by adjusting the optical constants of the layers. The experimental line width, $\Delta\theta$ (full-width at half-maximum) of the SPR curves for (a) Au/Co (8 nm)/Au/air, (b) Au/Co (4 nm)/Au/air and (c) Ag/Co (4 nm)/Au/air are 1.2 , 0.8 , and 0.6° , respectively and these give the quality factor, $Q_{SPR} = \Delta\theta_{SPR}/\theta$ as 46, 52 and 67, respectively (highest for the Ag/Co (4 nm)/Au/air configuration, denoted as Configuration B).

The shape of the reflectance curve (Lorentzian) in Figure 2 are determined by the mode propagation constant. The real and imaginary parts of the propagation constant can be determined by the SPR angle and resonance width as $\text{Re}[\beta] = k_0 n \sin(\theta_{SPR})$, and $\text{Im}[\beta] = 0.5 k_0 n \Delta\theta \cos(\theta_{SPR})$, respectively¹³. The fact that the Ag layer in the multilayer leads to a narrowing of the resonance in the reflectance curve, as indicated by the lower $\Delta\theta$ and higher Q-factor, is an indication of the lower optical losses (higher conductivity) of Ag. Using Ag for the inner plasmonic layer provides higher Q-factor, but cannot be used without an additional capping layer for the external plasmonic layer to avoid oxidation. The outer Au layer is in contact with the probing sample, in this case, air.

Figure 3 shows the transverse T-MOKE spectra obtained from the experiment. These spectra were obtained from the difference in reflectance curves measured using a CMOS matrix when the magnetic field was applied in

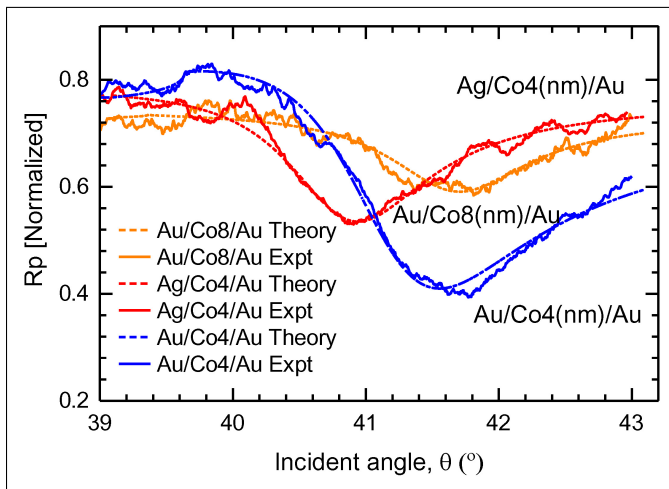


FIG. 2. p-polarization reflectivity profiles for the Ag- or Au-rich structures. Air is the probing medium. Dashed lines (theory) and solid lines (experiment).

the opposite directions as in¹³:

$$T - MOKE = 2 \times \frac{R_{p(+)} - R_{p(-)}}{R_{p(+)} + R_{p(-)}} \quad (1)$$

where $R_{p(+)}$ and $R_{p(-)}$ represent reflectance measured when the transverse H field is applied in the positive and negative directions, respectively. The characteristics of the measured Kerr effect strongly depend on the characteristics of the plasmon resonance and resonance width as well as variation of plasmon dispersion due to the opposing magnetic fields.

The magnitude of T-MOKE signal depends on the derivative of the reflectance curve as well as its absolute reflectance value. This means that the incident angle corresponding to the maximum T-MOKE spectra in Fig. 3 differs from the angle corresponding to maximum R_p spectra in Fig. 2.

The Q-factor of the sensing structure is crucially important both for SPR and MOSPR sensing, since the steeper the resonance is, the higher response is observed for the same variation of the analyte. The T-MOKE spectra in Fig. 3 shows a much smaller $\Delta\theta$ values for (a) Au/Co (8 nm)/Au/air, (b) Au/Co (4 nm)/Au/air and (c) Ag/Co (4 nm)/Au/air and they are 0.7, 0.45, and 0.32° respectively and these give the quality factor, Q_{MOSPR} , calculated as $Q_{MOSPR} = \Delta\theta_{MOSPR}/\theta$ as 95, 105 and 140, respectively (highest for the Ag/Co 4 nm/Au/air configuration). As shown in Figs. 2 and 3, there exists a small difference between the optimum working angles for the reflectance and T-MOKE measurements. In the case of T-MOKE measurements, the magnitude of the T-MOKE spectra is proportional to the derivative of the reflectance, which is highest for the steepest part of the reflectance curve. The various response parameters of reflectance and T-MOKE measurements are listed in Table I.

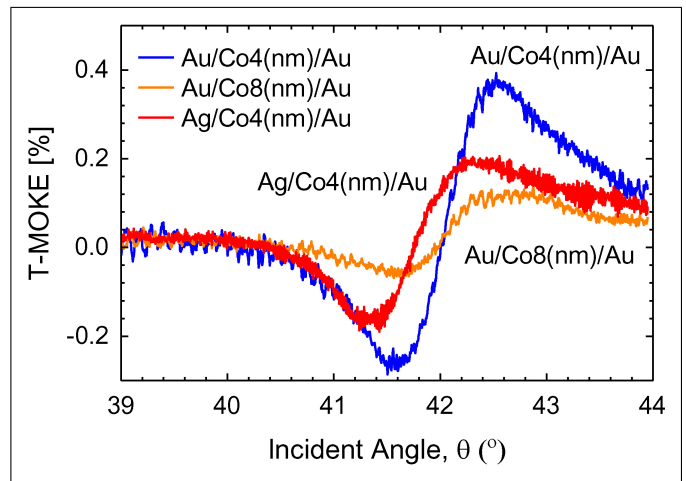


FIG. 3. T-MOKE profiles experimentally obtained using (1). Air is used as the probing medium.

The magneto-optic enhancement, together with the modulation provided by the alternating magnetization of the magnetic layer, leads to a drastic improvement of the quality factor (and thus the sensor sensitivity). As expected, a thicker Co layer leads to higher losses visible through a broader line shape, larger absorption at low incidence angles and lower reflectivity minimum¹¹. Comparing the signal to noise ratios of Figs. 2 and 3, it can be inferred that the T-MOKE measurement is more accurate and can yield a greater resolution in terms of the detectable variation in the probed refractive index. The higher noise observed for the R_p measurement is considered to be due to parasitic interference and the need for the normalization of the optical spectrum, whereas in the case of T-MOKE measurements, the absolute intensity of the reflected signal does not matter. This makes magneto-optical measurements more accurate than reflectivity. Further optimization of the sample, e.g. utilization of photonic crystals¹³, can lead to a narrowing of the resonances and therefore to the reduction in the noise level, so that even higher resolution in the measurement of the variations in the probed refractive index can be attained.

TABLE I. Optical properties of the fabricated sensors

Material	R_p		T-MOKE	
Sensor	FWHM	Q	FWHM	Q
Ti/Au/Co(8 nm)/Au	1.2	46	0.70	95
Ti/Au/Co(4 nm)/Au	0.8	52	0.45	105
Ti/Ag/Co(4 nm)/Au	0.6	67	0.32	140

The sensitivity of SPR and MOSPR biosensors is a critical parameter for their benchmarking. However, no unified sensitivity metric is used in the literature to directly compare the performance of these sensors. According to our sensitivity metrics, which allow direct compar-

TABLE II. Comparative Sensitivity Characteristics. *Denotes theoretical results using optical constants derived from the experiment, rather than the bulk values. PC: photonic crystal

Material (nm)	$S_{SPR}(\%/RIU)$		$S_{MOSPR}(\%/RIU)$		Result Type	Source
	632.8 nm	780 nm	632.8 nm	780 nm		
Au(50)	2.5×10^4	7.5×10^4	—	—	Theory	11
Cr(2)/Au(45)	6.7×10^4	—	—	—	Experiment	2
Cr(2)/Co(7.5)/Cr(3)/Au(23)	—	—	1.9×10^5	—	Experiment	2
PC/Co(10)/Au(9)	—	1.2×10^5	—	7.5×10^5	Theory	13
PC/Co(10)/Au(9)	—	9.0×10^4	—	3.0×10^4	Experiment	13
Ta/Co(8)/Au(35)	1.6×10^4	2.1×10^5	4.0×10^4	2.2×10^5	Theory	11
Ta/Co(4)/Au(35)	—	—	—	5.7×10^5	Theory	11
Ta/Co(8)/Ag(35)	5.2×10^4	3.3×10^5	8.0×10^4	8.0×10^5	Theory	11
Ta/Co(4)/Ag(35)	—	—	—	2.5×10^6	Theory	11
Ti/Ag(35)/Co(4)/Au(10)	6.0×10^2	1.0×10^4	1.1×10^4	3.0×10^4	Theory*	[This work]

ison of the response of SPR and MOSPR devices^{8,11}, the SPR and MOSPR sensitivities to measuring changes during an air to Helium transition in the probed environment are defined as:

$$S_{SPR} = \frac{[R_{p(air)} - R_{p(He)}]}{\Delta R_{p(air)m}} \times 100 [\%/RIU] \quad (2)$$

and

$$S_{MOSOR} = \frac{[\Delta R_{p(air)} - \Delta R_{p(He)}]}{\Delta R_{p(air)m}} \times 100 [\%/RIU] \quad (3)$$

respectively, where, $R_{p(air)m}$ is the magnitude of the reflected intensity at an incident angle θ_m , where the slope of the reflectivity curve is maximum, and $\Delta R_{p(air)m}$ is defined similarly at the point of maximum slope of the T-MOKE response. The Δn in (2) and (3) is the difference in refractive indices between air and Helium media, and RIU denotes refractive-index-unit.

Table II summarizes representative literature sensitivity values for both theory and experimental results, including the results of this work. MOSPR responses are systematically superior to SPR structures, and Ag-based structures lead to higher sensitivity due to lower losses. The enhancement with Ag is independent of wavelength as the Ag conductivity is better than that of Au in this frequency range. Longer wavelengths typically lead to higher losses and shorter wavelengths lead to cross-over of the real part of the dielectric permittivity to positive values, where plasmon resonance no longer takes place. The experimental sensitivities often lag theoretical predictions, but that in most cases is due to sub-optimal device fabrication or material quality.

Fig 4 shows a comparison of the modeled SPR and MOSPR sensitivities of the Ag-rich sensor (Ti/Ag/Co(4nm)/Au) calculated using (2) and (3) and the refractive indices obtained from the experiment for this sensor configuration. The modeled transition between air and He in the probed medium is indicative of the relative response of the sensors. Due to the small difference in refractive indices between air and He ($\sim 10^{-4}$

RIU), the change in gas medium does not affect the resonance width or depth. The modeled sensitivity of the MOSPR sensor shows an improvement by 3X over the SPR sensor, and this can be further improved by suitably modifying the configuration.

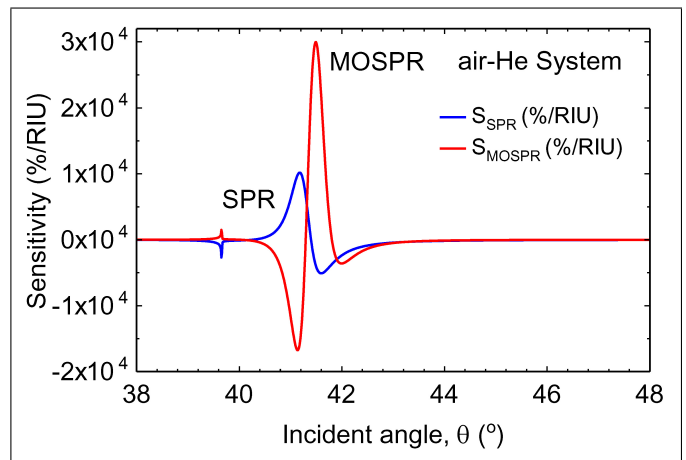


FIG. 4. SPR (reflectivity vs. incident angle) sensitivity vs. MOSOR (change in reflectivity due to the presence of a saturating magnetic field H vs. incident angle) sensitivity of a Ti/Ag/Co(4 nm)/Au sensor expressed in (%/RIU). Blue line (SPR) and red line (MOSPR).

IV. CONCLUSIONS

We presented two types of surface plasmon resonance configurations based on 4 or 8 nm of Co and Au vs. Ag layers and obtained the quality factor for two plasmonic sensing schemes (SPR vs. T-MOKE). While the ferromagnetic Co introduces some losses for the SPR spectra, the T-MOKE response overrides this loss¹³. Magneto-optical non-reciprocity becomes more significant in these structures leading to an increase in the magnitude of the transverse Kerr effect and thus, the Q-factor.

The advantage of the T-MOKE sensor over the existing SPR based sensors is significant. The new sensor shows improvement of Q-factor by over 2X of that of SPR. The magnetic field also has the added benefit that as opposed to measuring the angular shift of the SPR signal as it is typically done, it allows measuring the change in intensity of the reflected light. The MOSPR sensitivity of the sensor obtained using our sensitivity metrics shows an improvement by 3X over the SPR sensitivity. The ease of measuring changes in reflectivity and enhancement in Q-factor makes the T-MOKE based sensors currently being developed advantageous over the existing SPR sensors presently available on the market, to potentially allow T-MOKE sensors to probe bio-samples having much lower analyte concentrations. This work experimentally demonstrates the enhanced sensitivity of the magneto-optic structure as a potential biosensor.

V. ACKNOWLEDGMENT

We would like to acknowledge CMC Microsystems for the provision of products and services that facilitated this research, including access to COMSOL Multiphysics and funding provided for sample fabrication at the Micro-fabrication Laboratory, Polytechnique Montréal, Canada (Grants # 5357). The work of D.O.I., P.O.K. and V.I.B. was supported by Russian Foundation for Basic Research (Grants # 18-52-80038 and 18-52-45021).

VI. REFERENCES

- ¹A. K. Zvezdin and V. A. Kotov, *Modern magneto-optics and magneto-optical materials* (CRC Press, 1997).
- ²B. Sepúlveda, A. Calle, L. M. Lechuga, and G. Armelles, “Highly sensitive detection of biomolecules with the magneto-optic surface-plasmon-resonance sensor,” *Optics letters* **31**, 1085–1087 (2006).
- ³B. Diaz-Valencia, J. Mejía-Salazar, O. N. Oliveira Jr, N. Porrás-Montenegro, and P. Albella, “Enhanced transverse magneto-optical kerr effect in magnetoplasmonic crystals for the design of highly sensitive plasmonic (bio) sensing platforms,” *ACS omega* **2**, 7682–7685 (2017).
- ⁴D. O. Ignatyeva, G. A. Knyazev, P. O. Kapralov, G. Dietler, S. K. Sekatskii, and V. I. Belotelov, “Magneto-optical plasmonic heterostructure with ultranarrow resonance for sensing applications,” *Scientific reports* **6**, 28077 (2016).
- ⁵G. Pellegrini and G. Mattei, “High-performance magneto-optic surface plasmon resonance sensor design: an optimization approach,” *Plasmonics* **9**, 1457–1462 (2014).
- ⁶G. Armelles, A. Cebollada, A. García-Martín, and M. U. González, “Magnetoplasmonics: combining magnetic and plasmonic functionalities,” *Advanced Optical Materials* **1**, 10–35 (2013).
- ⁷D. Regatos, B. Sepúlveda, D. Fariña, L. G. Carrascosa, and L. M. Lechuga, “Suitable combination of noble/ferromagnetic metal multilayers for enhanced magneto-plasmonic biosensing,” *Optics express* **19**, 8336–8346 (2011).
- ⁸C. Rizal, V. Belotelov, D. Ignatyeva, A. K. Zvezdin, and S. Pisana, “Surface plasmon resonance (SPR) to magneto-optic SPR,” *Condensed Matter* **4**, 50 (2019).
- ⁹C. Rizal and V. I. Belotelov, “Sensitivity comparison of surface plasmon resonance (SPR) and magneto-optic SPR biosensors,” *Eur. Phys. J. Plus* **134**, 7 (2019).
- ¹⁰C. Rizal, “Magneto-optic surface plasmon resonance Ti/Au/Co/Au/Pc configuration and sensitivity,” *Magnetochemistry* **4**, 35 (2018).
- ¹¹C. Rizal, S. Pisana, and I. Hrvoic, “Improved magneto-optic surface plasmon resonance biosensors,” *Photonics* **5**, 15 (2018).
- ¹²M. H. H. Hasib, J. N. Nur, C. Rizal, and K. N. Shushama, “Improved transition metal dichalcogenides-based surface plasmon resonance biosensors,” *Condensed Matter* **4**, 49 (2019).
- ¹³D. Ignatyeva, P. Kapralov, G. Knyazev, S. Sekatskii, G. Dietler, M. Nur-E-Alam, M. Vasiliev, K. Alameh, and V. Belotelov, “High-q surface modes in photonic crystal/iron garnet film heterostructures for sensor applications,” *JETP letters* **104**, 679–684 (2016).
- ¹⁴M. Schubert, T. E. Tiwald, and J. A. Woollam, “Explicit solutions for the optical properties of arbitrary magneto-optic materials in generalized ellipsometry,” *Applied optics* **38**, 177–187 (1999).
- ¹⁵P. Johnson and R. Christy, “Optical constants of transition metals: Ti, V, Cr, Mn, Fe, Co, Ni, and Pd,” *Physical review B* **9**, 5056 (1974).